ELSEVIER

Computers & Geosciences 30 (2004) 461–469

COMPUTERS & GEOSCIENCES

www.elsevier.com/locate/cageo

New discrimination techniques for Euler deconvolution

Desmond FitzGerald[a,*], Alan Reid[b], Philip McInerney[a]

[a] *Intrepid Geophysics, Unit 2, 1 Male Street, Brighton, Victoria 3186, Australia*
[b] *Reid Geophysics, University of Leeds, UK*

Received 18 August 2003; received in revised form 24 February 2004; accepted 12 March 2004

Abstract

Euler deconvolution has come into wide use as an aid to interpreting profile or gridded magnetic survey data. It provides automatic estimates of source location and depth. In doing this, it uses a structural index (SI) to characterise families of source types.

Euler deconvolution can be usefully applied to gravity data. For simple bodies, the gravity SI is one less than the magnetic SI. For more complex bodies (including the contact case), the Euler method is at best an approximation. Extended Euler provides better-constrained solutions for both gravity and magnetic bodies.

Seven alternative formulations on the extended Euler equations are presented. A parametric model study for extended Euler reveals the ability to calculate depths, SI, strike and error estimates. The computed SI values from model studies are compared to equivalent examples from field data across known geological structures.

New discrimination techniques for isolating geological bodies of interest are proposed and applied. The computed SI is used to discriminate magnetic signatures arising from known kimberlites. In another study, the discrimination is used to classify major fault contacts. The advent of new formulations of Euler equations offers scope to further refine discrimination strategies.

Keywords: Depth; Hilbert; Structural index; Extended; Inclination

1. Theory

Euler deconvolution is only valid for homogeneous functions. A function $f(\mathbf{v})$ of a set of variables $\mathbf{v} = (v_1, v_2,...)$ has a degree of homogeneity n, if

$$f(t\mathbf{v}) = t^n f(\mathbf{v}), \tag{1}$$

where t is a real number. If f has a differential at $\mathbf{v}$, then

$$\mathbf{v}\,\nabla_{\mathbf{v}} f(\mathbf{v}) = nf(\mathbf{v}). \tag{2}$$

This is Euler's equation, and Euler deconvolution relies on solving it in appropriate cases. A field f, which may be expressed in the form

$$F = A/r^{-N} \tag{3}$$

will be homogeneous of degree $-N$. For convenience we define the structural index (SI) as N ($=-n$, i.e. the negative degree of homogeneity).

Thompson (1982) showed that Euler's equation could usefully be written in the form

$$(x - x_o)\partial T/\partial x + (y - y_o)\partial T/\partial y + (z - z_o)\partial T/\partial z = N(B - T), \tag{4}$$

where (x_o, y_o, z_o) is the position of a magnetic source whose total field T is detected at (x, y, z). The total field has a regional value of B. N is the SI.

*Corresponding author. Tel.: +61-3-9593-1077; fax: +61-3-9592-4142.

E-mail addresses: des@dfa.com.au (D. FitzGerald), alan@reid-geophys.co.uk (A. Reid), phil@dfa.com.au (P. McInerney).

0098-3004/$ - see front matter © 2004 Elsevier Ltd. All rights reserved.
doi:10.1016/j.cageo.2004.03.006

This is recast by Nabighian and Hansen (2001) in the following form:

$$(x-x_o)\partial T/\partial x+(y-y_o)\partial T/\partial y+(z-z_o)\partial T/\partial z + N(T-B)=\alpha, \quad (5)$$

where α is a constant which normally vanishes except for $N=0$.

The Extended Euler (Mushayandebvu et al., 2001; Nabighian and Hansen, 2001) follows from the observation that potential fields are also invariant under rotations. This leads to two new equations for the 3D case. A distinction is made between a Hilbert Transform in the local East or X direction and the local North or Y direction.

$$(x-x_o)\partial(\boldsymbol{H}_x(T))/\partial x+(y-y_o)\partial(\boldsymbol{H}_x(T))/\partial y + (z-z_o)\partial(\boldsymbol{H}_x(T))/\partial z+N\boldsymbol{H}_x(T)=\beta_x, \quad (6)$$

$$(x-x_o)\partial(\boldsymbol{H}_y(T))/\partial x+(y-y_o)\partial(\boldsymbol{H}_y(T))/\partial y + (z-z_o)\partial(\boldsymbol{H}_y(T))/\partial z+N\boldsymbol{H}_y(T)=\beta_y, \quad (7)$$

where β_x and β_y are constants which normally vanishes except for $N=0$.

Thus, if a solution of Laplace's equation satisfies an Euler equation with index N, so do its generalised Hilbert transforms. By applying Hilbert transforms, a circular rotation of the coordinate axes is achieved. All equations are valid as the Hilbert directional transforms are locally independent of each other and the original field.

The Extended Euler work also shows α and β_x and β_y as being derivable from body properties for more than the contact case. We therefore carry these throughout for generality. The regional B also requires further investigation. As shown in the Eq. (5), B is assumed to be a local constant. This is not the only possibility, and B could be formulated as varying. For the purposes of this study, using a regional B and α in Eq. (5) is not pursued formally. For the majority of this study, α is used as a catch all and no B term is used. Also, β_x and β_y are treated as one common factor β. This point is presently unresolved and offers scope for further research.

2. Practical considerations

There are up to eight unknowns or degrees of freedom in the above equations. These are the X, Y, Z vector offset from the observed field position to the causative body, N the SI or rate of fall-off of the power, the local background of the field and three material property factors that may or may not be present for the non-contact case. This assumes that locally the observed field is being induced by just one body. The case of the local field being induced by two bodies has been presented by Hansen and Suciu (2002) and Hansen (2002) for the Werner 3D grid variation and requires that each body have the same N. This case is not pursued in this paper.

The formulation of an Euler code can either use α or the Background term but not both.

Also, it is assumed that $\beta_x = \beta_y$ for this study.

Seven variations on the equations have practical significance. These are quoted below and the variables to be solved for are shown for each case.

(1) Traditional Euler only (Eq. (5)); solve for X, Y, Z and B.
(2) Two Hilbert equations only (Eqs. (6) and (7); pure rotational invariance of a homogenous field); solve X, Y, Z, N and β (assume $\beta_x-\beta_y$).
(3) Three equations (Traditional and two Hilbert; Eqs. (5)–(7) but assume a fixed SI; solve X, Y, Z and B.
(4) Three equations with 6 unknowns; solve X, Y, Z, N, α and β (assume $\beta_x-\beta_y$).
(5) Three equations, with a reduction to two equations, substituting out the SI (basement solver case); solve X, Y, Z, α and β.
(6) Three equations but assuming that we also have a continuous *known* depth to basement. This is an inversion for body *properties* of the basement, and for any intrusives in the basement; solve N, α and β.
(7) Use three equations after first spatially locating a 2D body by edge picking techniques; solve Z, N, α and β.

3. Solution strategy

The traditional Euler approach uses a convolution window (5–10 grid-cells square) and forms 25–100 equations for the four unknowns. Conventional wisdom is to make the convolution width not less than half the maximum depth to required sources. The equations are solved by a least squares, singular value decomposition. The traditional Euler deconvolution has a history of producing *sprays* of solutions, within which the correct answer for each discrete body needs to be found.

With three equations, there are now 75–300 observations in up to 6 unknowns. There are usually an abundance of observation points of the field so the system of equations is over determined and weighted least squares minimises the errors in the solution for best fit and also yields extensive local error estimates.

The traditional method that allows error estimation and minimisation remains the preferred approach. Solutions for combinations of the vector to source position, the SI, background and property indicators (alpha and beta) are now routinely possible.

The additional equations provide better-behaved clustering of solution positions, with more accuracy

and less *sprays* (source location *errors*). Although the problems of *sprays of solutions* is much reduced, there is still a requirement for intelligent analysis of clusters of solutions, and culling of poor solutions. The extra equations do, however, provide new opportunities to advance this intelligent analysis, selection and culling of solutions.

An alternative to the least squares approach is possible for the case of $N > 0$, and fixed in value (say, 1), and no background. There are three equations in three unknowns, and an explicit solution can be derived for every point location. Each observational point stands on its own merits and has no interference from its neighbours. This is rarely achieved in practice, especially where the *estimation* of gradients is required. New gravity and magnetic gradiometry acquisition systems, specifically *measuring* gradients, promise to meet this ideal. (Zhang et al., 2000).

4. Structural index

The SI can be interpreted as the integer exponent in a power law expressing the fall-off of field strength versus distance from source. For magnetic data, physically plausible SI values range from 0 (contact of infinite depth extent) to 3 (point dipole). Values less than 0 imply a field strength that *increases* with distance from source (and is infinite at infinity). Values greater than 3 imply quadruple or higher-order multiple sources.

The value of the SI is important, because use of the wrong value leads to the calculation of misleading depths, with errors more than twice the depth at times. But there seems to be a problem in the gravity case. Stavrev (1997) gives an admirably complete and closely argued analysis of the problem, showing that the gravity SI for any given structure should simply be one less than the equivalent magnetic value.

The derived values shown in Table 1 are from Reid et al. (2003; 1990), and Reid (2003).

A difficulty arises for the gravity contact case because the simple rule leads to a value of -1.0 This is theoretically awkward because it implies an *increase* in the gravity field strength with distance from the source, reaching infinite value at infinity. Hence, the introduction of two extra terms (α and β) for the contact case to handle this problem. Even then, it is an approximation.

Other possible sources, such as large steps, give rise to fields which are not strictly homogeneous. Furthermore, *real* geological bodies (e.g. kimberlite pipes) are more complex than simple model bodies, and thus the application of Euler deconvolution to real data is always an approximation.

Table 1
SI for gravity and magnetics

Source	Gravity SI	Magnetic SI
Sphere	2	3
Horizontal cylinder	1	2
Fault (small step)	0	1
Contact	−1	0

5. Discrimination techniques

A discrimination technique is needed to distinguish more reliable solutions from spurious ones, and to characterise geological features of interest. Traditional discrimination techniques for grid Euler are:

(1) Rejection of estimated *depth error*/*depth* greater than, say, 50%.
(2) Solutions falling outside the convolution window width.
(3) Solutions falling outside the observed survey data. (This is not strictly necessary as near misses to an edge may be valid solutions.)
(4) Signal strength of the anomaly being less than some specified threshold.
(5) Spatial binning of solutions, and selecting the best solutions in each bin based on a Laplacian or signal strength criterion.
(6) Low pass filtering of the data to constrain the frequency content.
(7) Rejection of solutions based on *reliability*.

Suggested new techniques are:

(8) Rejection of bodies that have inadmissible SI.
(9) Rejection of bodies that have SI values that are of no interest to the interpreter.
(10) Rejection of bodies that have a singularity ratio that is too large or too small if searching for 2D bodies.
(11) Co-variance of the X Y equations in a convolution window being too high.
(12) Rejection of bodies that have too high an SI error.
(13) Solution rejection based on histogram analysis of various parameters of the local population (e.g. skewness and kurtosis of the reported depths of the local population).
(14) Analysis of the *clustering* of solutions. The deconvolution process yields many similar or duplicate solutions, which may be tightly clustered in the vicinity of real sources.
(15) Rejection of solutions where the vector from the observed point to the causative body has a inclination or dip that is too low.
(16) Rejection of solutions where the α and β values are not close to 0.0, especially for higher SI values.

(17) Downward continuation of data for a sedimentary basin setting, to enhance the signatures of deep basement structures.

6. Singularity ratio

In the singular value decomposition least-squares technique, each degree of freedom has a singularity weight. This singularity weight is the least squares weight that is fundamental to the method. The singularity ratio is calculated by finding the ratio of the maximum singularity weight to the minimum. Often the components involved are for the X and Y and thus relate to body geometry.

Mushayandebvu et al. (2003) note that using the 3D formulation on 2D bodies can lead to the failure of the deconvolution process, or result in poorly constrained solutions. All model studies involving 2D bodies, show only a relatively small instability in the singularity ratio, nowhere near the instability floor of 10^{-6}. Typically, the ratio is in the range 50–300 for magnetics, and 5000 for gravity. Comparable values are observed for real data comprising dyke swarms. This observation provides a useful discrimination for both cluster reductions and deciding what equations to use to infer the dip and susceptibility or density of the bodies.

As you allow for more degrees of freedom, the singularity ratio is observed to increase. Thus, when solving for the alpha and beta terms, the singularity ratio is at its most extreme.

7. Reliability

The reliability is another measure derived from the singular value decomposition. This factor is calculated by taking either the *trace* of the singularity weights, or the *product* of those weights. The maximum reliability value (for the entire dataset) is used to *scale* all reliability values, yielding a number between 0 and 1. Since this is a highly skewed population, the values are regularized by computing the square root. Given the recent work on singularity ratios, this quantity not only reflects the power of the anomaly signal, but is dominated by the X and Y uncertainties for 2D bodies. It has proven effective in identifying (and culling) poorer solutions.

8. Inclination angle

The deconvolution process involves inferring from the induced field a family of discrete causative bodies. Three important quantities typically being solved for in the Euler equations are the X, Y and Z offsets from the current observation point to the causative source. The *inclination* (or dip) of this (X, Y, Z) vector combines these three quantities in one term, and may be used as a primary tool in both discrimination and fine-tuning. Solutions with low inclination may be regarded as suspect.

9. Error estimation techniques

Error estimation is based on Gaussian assumptions, and even allowing for scaling by the Structural Index (Thompson, 1982), *these errors do not properly reflect the real errors* observed in model studies. The Z error term in particular has been used traditionally, but results from this study indicate that it may be misleading. One explanation offered is that typical potential field datasets have considerable *correlation* between neighbouring observations, thus violating a basic assumption of elementary statistics viz. that all observations are *independent*.

There are two simple ways of investigating this:

(1) A co-variance estimate for X, Y and Z parameters. These follow the normal principals and are presented in all the tables. The quantities XY_err, YZ_err, ZSI_err represent the cross correlation of individual terms with each other. Surprisingly, the cross correlations are extremely small except for the case of a relatively small grid cell size and a large convolution kernel for a 2D body. This shows up in the XY_err term. Whilst the Depth/SI cross correlation was not tabulated, the gravity contact case study shows a link between these quantities.
(2) A second test is that of using a Newton–Raphson method of improving the estimated error. Tests have shown that the improvement from this approach is less than engineering accuracy, and of no value.

10. Model studies

10.1. Contact model

The new formulations of Euler equations have been applied to grids of magnetics and gravity computed for several simple models. The example illustrated here (Fig. 1) is the Fault Contact case, which may be compared to the field example in Fig. 5. The equations for case 2 (two Hilbert equations) directly solve for SI, as well as strike, X, Y and Z. Note that the computed SI for the magnetic case is 1, and for the gravity case is 0.7.

10.2. Combination model—sphere, horizontal cylinder, vertical pipe

The first six of the seven proposed formulations of the Euler equations have been implemented. These

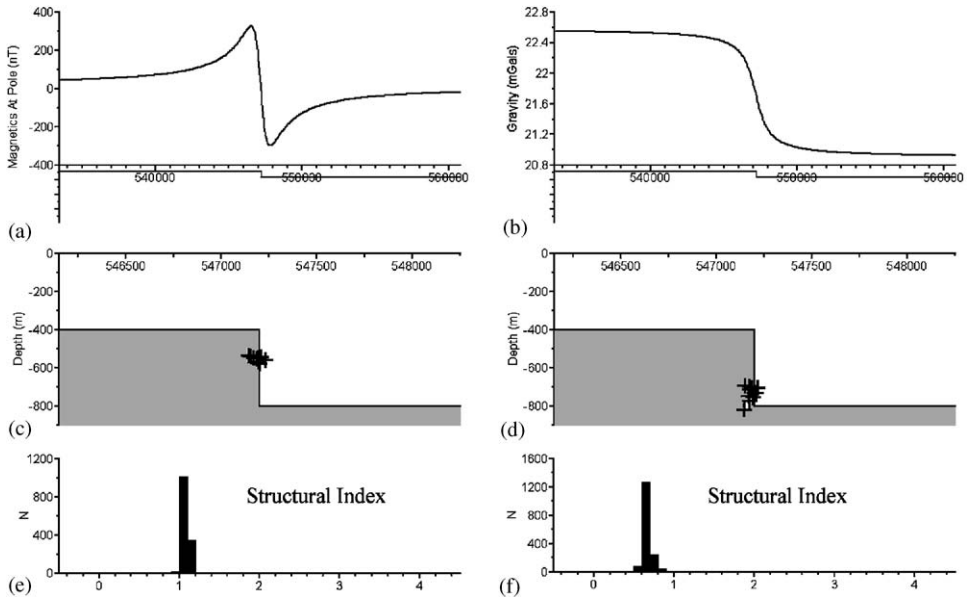

Fig. 1. Plot of depth solutions from Euler deconvolution (two Hilbert equations case) of modeled magnetics at pole (a) and gravity (b) for a fault contact model. Top of step model was 400 m, bottom 800 m, contact vertical, oriented N030°E. Computed Structural Index (SI) is 1 for the magnetic case (e), and 0.7 for gravity (f). Solutions do plot on contact, but computed depths (c, d) do not accurately predict either top or bottom of contact.

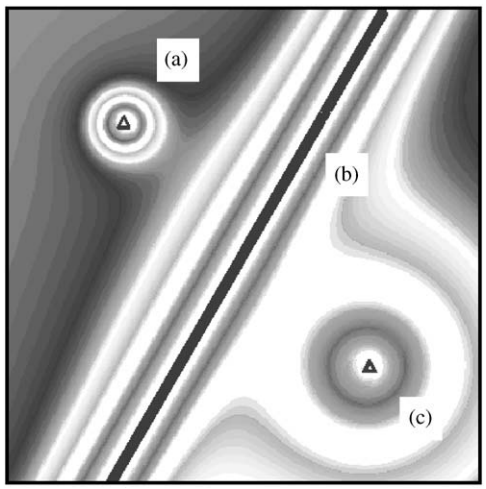

Fig. 2. Computed gravity image for combination model of sphere (a), horizontal cylinder (b) and vertical pipe (c). Solutions from Euler deconvolution (two Hilbert equations case) are plotted as triangles. This model was used as a basis for comparison of solutions from various alternative formulations of Euler equations (Tables 3, 4).

formulations have been tested for both the magnetics and gravity cases using a model dataset generated from a combination of three simple models—a sphere, a horizontal cylinder, and a vertical pipe (Fig. 2, Table 2). In order to rapidly assess the strengths and weaknesses of each formulation, and to directly compare results,

Table 2
Properties for combination model grid

Body type	Depth	SI (Mag)	SI (Grav)
Sphere	500	3	2
Horizontal cylinder	400	2	1
Vertical pipe	250	2	1

solutions have been computed at three selected points near to the top of each body. The full results are presented in Table 3 (magnetics) and Table 4 (gravity). For each formulation, the three rows of the tables correspond to the result from points located over the sphere, the horizontal cylinder, and the vertical pipe, respectively. Note that for some formulations, certain parameters are specified inputs. Also, some formulations solve for only a subset of the parameters; parameters not computed are shown as '—'.

10.3. Combination model—magnetics case: comparison of alternative Euler formulations (Table 3)

In general, for these simple model cases, most formulations yield results close to expected values. Those formulations which solve for SI all work very well and yield very accurate results. For those cases that *assume* a fixed SI (set to 2), the depths for the *sphere* are underestimated, as expected. The Z depth of the vertical

Table 3
Comparison of parameters derived from alternative formulations of Euler equations. (Combination Model, Magnetics Data; 160 m grid cell size, magnetics at pole)

X	*Y*	*Z*	*BG*	*X*err	*Y*err	*Z*err	*BGer*	*Rel*	*Strk*	SI	SI_err	*XY*_err	*YZ*_err	*SRat*	alpha	beta
Classic Euler																
540245	6466369	−307	−3.53	0.67	0.64	0.40	0.053	1.0000	91	2	—	6.14E−09	1.27E−07	21.6	—	—
546876	6458838	−401	0.00	34.3	59.4	0.49	0.053	0.5612	−146	2	—	7.96E−02	1.41E−05	142.7	—	—
554194	6452401	−228	−1.00	0.49	0.49	0.35	0.051	1.0958	−82	2	—	2.62E−08	1.12E−07	23.9	—	—
Hilbert Equations only																
540200	6466400	−499	—	0.67	0.68	1.22	—	1.0000	−163	3.00	0.0065	5.63E−07	6.20E−06	39.9	—	0.420
546471	6458138	−403	—	34.7	60.0	1.01	—	0.6044	30	2.01	0.0043	8.13E−02	5.34E−05	253.6	—	−0.061
554187	6452403	−261	—	0.51	0.52	0.82	—	1.1294	−144	2.25	0.0053	7.56E−08	1.82E−06	45.3	—	−0.661
All 3 equations, assuming a fixed SI of 2																
540235	6466372	−315	−3.93	0.47	0.46	0.30	0.051	1.0000	92	2	—	2.00E−07	2.49E−07	38.9	—	0.611
546668	6458477	−400	0.00	24.8	42.9	0.35	0.052	0.5657	−146	2	—	4.15E−02	6.01E−06	143.3	—	−0.006
554192	6452400	−227	−0.98	0.35	0.35	0.24	0.050	1.0978	−81	2	—	3.12E−08	9.53E−09	46.9	—	−0.460
All 3 equations, with full 6 degrees of freedom																
540200	6466400	−500	—	0.49	0.48	0.94	—	1.0000	92	3.00	0.0048	6.65E−07	4.34E−06	93.1	−1.177	0.425
546667	6458477	−402	—	24.8	42.9	0.79	—	0.5869	−146	2.01	0.0036	4.15E−02	1.57E−06	251.7	0.012	−0.041
554190	6452402	−263	—	0.35	0.36	0.56	—	1.1402	−81	2.26	0.0035	2.44E−09	4.86E−07	105.6	1.873	−0.618
Basement formulations, with no calculation of SI																
540202	6466401	−501	—	0.01	0.01	0.02	—	1.0000	92	—	—	4.10E−09	2.13E−11	328.5	0.882	−1.351
546564	6458300	−402	—	0.31	0.54	0.02	—	0.6291	−146	—	—	6.66E−06	3.03E−08	373.8	−0.031	0.074
554185	6452393	−315	—	0.01	0.01	0.01	—	1.2480	−81	—	—	8.95E−10	2.59E−11	329.5	−19.67	6.587
Known source location case, solve for properties																
540200	6466500	−500	—	—	—	—	—	1.0000	92	3.14	0.0015	—	—	71.6	−6.044	1.101
546500	6458400	−400	—	—	—	—	—	1.0026	−146	2.18	0.0015	—	—	68.9	−7.850	−0.643
554000	6452500	−250	—	—	—	—	—	0.9972	−81	2.25	0.0015	—	—	72.9	−2.731	−0.120

Abbreviations: BG Background; BGer Background error; Rel Reliability; Strk Strike; Inclin Inclination; SRat S_Ratio.

pipe has the largest error and the estimated error for this quantity is consistently underestimated.

The horizontal cylinder shows the biggest singularity ratio and also the largest X and Y errors. This is not unexpected. The α and β terms, if calculated, are a better indicator of error than the least-squares error estimates. The last equation case illustrates this well. The observation point chosen as being top dead centre of the bodies is actually slightly in error and the alpha reflects this very well.

10.4. Combination model—gravity case: comparison of alternative euler formulations (Table 4)

For this case, not all formulations gave a valid solution. The least squares error estimates are much larger than for magnetics. Isolated, small gravity bodies are more difficult to detect due to typically lesser signal strength, and a larger operator is recommended. When one of the degrees of freedom is constrained, the equations work much more reliably. For example, magnetic can be regarded as a directional derivative of gravity, has a faster decay rate, and thus has a higher lateral resolution than gravity. Given the source geometry, magnetic produces a more accurate and reliable solution than does gravity.

11. Case history studies

11.1. Kimberlite study—high structural index case

The Sheoak Hill area, South Australia was explored for diamonds by Stockdale Prospecting in the early 1990s. Aeromagnetics was used to identify potential kimberlite targets (Fig. 3a). Subsequent drilling confirmed kimberlites, albeit barren of diamonds. Applying the Euler deconvolution to this grid dataset—and plotting *all* solutions, *without any* of the traditional discrimination techniques—resulted in an overwhelming 78 000 solutions for this small project area. Many solutions are very shallow, due to high frequency (noise ?) in the gridded data.

Table 4
Comparison of parameters derived from alternative formulations of Euler equations. (Combination Model, Gravity Data; 160 m grid cell size)

X	*Y*	*Z*	*BG*	*X*err	*Y*err	*Z*err	*BGer*	*Rel*	*Strk*	SI	SI_err	*XY*_err	*YZ*_err	*SRat*	alpha	beta
Classic Euler																
540318	6466303	−220	−0.03	245	236	131	0.073	1.0000	−86	1	—	3.86E−02	1.09E−01	23.1	—	—
546859	6458796	−399	0.02	46K	80K	149	0.084	0.4917	−150	1	—	1.44E+05	7.02E+00	8664	—	—
554199	6452400	−214	−0.01	225	220	137	0.074	1.0115	−85	1	—	5.00E−02	1.81E−02	21.2	—	—
Hilbert equations only																
540185	6466427	−573	—	229	232	407	—	1.0000	−178	2.47	1.4534	1.98E−01	9.96E−01	62.9	—	0.024
545301	6456134	−438	—	35K	61K	243	—	0.6092	30	1.12	0.4461	8.49E+04	1.19E+02	9405	—	−0.006
554218	6452384	−202	—	220	222	230	—	1.1192	−172	0.92	0.6067	5.39E−02	3.92E−02	32.1	—	−0.006
All 3 equations, assuming a fixed SI of 1																
540289	6466326	−210	−0.03	161	160	102	0.070	1.0000	−86	1	—	2.34E−02	6.44E−02	21.6	—	0.011
543276	6452586	−391	0.02	27K	47K	99	0.074	0.5097	−150	1	—	4.96E+04	1.71E+01	7180	—	−0.010
554207	6452393	−218	−0.01	156	156	102	0.070	1.0058	−85	1	—	8.67E−03	1.83E−02	20.8	—	−0.007
All 3 equations, with full 6 degrees of freedom																
540190	6466413	−537	—	181	176	293	—	1.0000	−86	2.21	1.0142	2.13E−01	7.22E−01	46.4	0.031	0.021
545589	6456641	−432	—	28K	49K	179	—	0.5764	−150	1.11	0.3793	5.43E+04	6.69E+01	7524	0.037	−0.004
554209	6452392	−206	—	158	157	178	—	1.0955	−85	0.96	0.5122	1.20E−02	1.01E−01	25.9	−0.015	−0.006
Basement formulations, with no calculation of SI																
540174	6466431	−515	—	582	586	1162	—	1.0000	−86	—	—	9.68E+00	4.39E+00	29.5	−0.053	−0.020
546559	6458300	−405	—	71K	100K	464	—	0.7490	−150	—	—	3.42E+05	1.04E+01	5415	−0.031	0.000
554214	6452385	−226	—	355	357	532	—	1.2827	−85	—	—	2.07E+00	5.23E−01	17.3	0.014	0.007
Known source location case, solve for properties																
540200	6466500	−500	—	—	—	—	—	1.0000	−86	2.24	0.3274	—	—	7	0.016	0.023
546500	6458400	−400	—	—	—	—	—	1.0734	−150	1.14	0.1858	—	—	4	0.013	−0.003
554000	6452500	−250	—	—	—	—	—	1.0151	−85	1.16	0.2905	—	—	6.3	−0.021	−0.006

Abbreviations: BG Background; BGer Background error; Rel Reliability; Strk Strike; Inclin Inclination; SRat S_Ratio.

For pipe-like bodies (kimberlites), the expected Structural Index value for magnetics is 2. Examination of the statistics of the computed SI shows that only a very small percentage of the solutions have an SI greater than 1. Using SI as a simple discriminator, and plotting only those solutions with an SI $>$ 1 (Fig. 3e) reveals a much more effective result. The four known kimberlites are identified with tight clusters of solutions, and there are also a modest number of other potential targets. Examination of those solutions within each of the pipes also showed that the depth to the pipes predicted by the Euler processing agreed well with drilling data.

11.2. Basin study— fault contact case

The Renmark Trough is an Early Permian Basin, which underlies the Tertiary Murray Basin in eastern South Australia. Seismic studies, and limited drilling confirm a sedimentary basin with some 2000–3000 m of non-marine and marine sediments. The main basin, and a bounding fault along the northern margin (Hamley Fault) are delineated by a low in the Bouguer Gravity Anomaly image (Fig. 4). A section through the Renmark Trough is presented in Fig. 5, together with Euler solutions, classified on the basis of their computed SI value. Again, in this example, all solutions have been plotted. As in the model study work presented above, solutions appear to be clustered at structural discontinuities. By classifying the solutions on the basis of computed SI, it is proposed that improved discrimination is achieved, and that major structural discontinuities can be identified as those with consistently higher structural Index values. Lower SI values may be indicative of lesser density anomalies, or may represent poorer solutions which should be ignored.

12. Discussion

12.1. Noise

Stability of solving is critically dependent on high-frequency noise in the calculated or observed gradients.

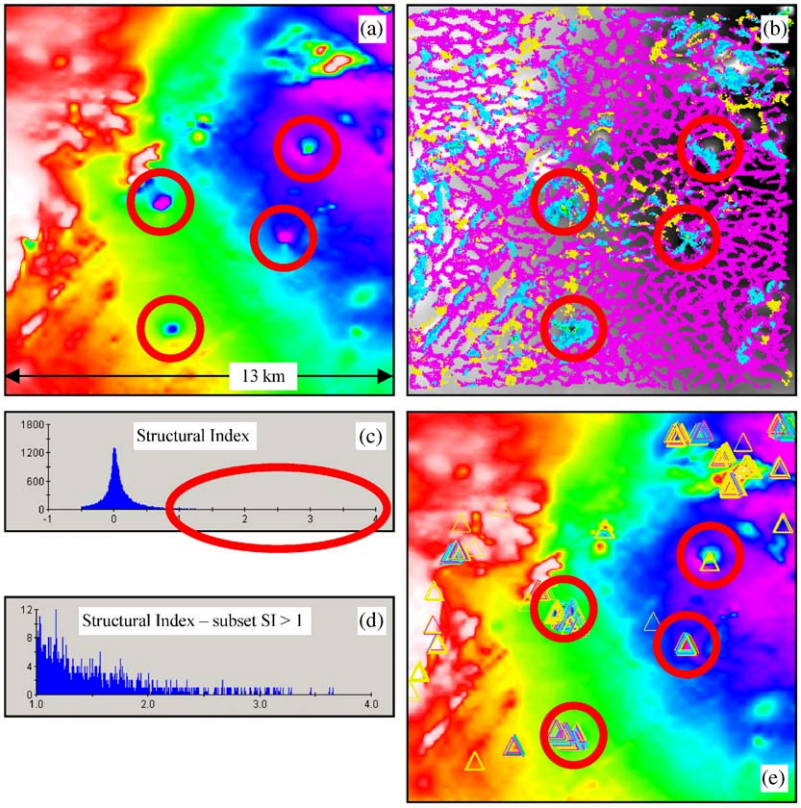

Fig. 3. Image of total magnetic intensity for Sheoak Hill, South Australia, showing magnetic signatures of four drilled (barren) kimberlites (a). Solutions from Euler deconvolution (two Hilbert equations case) are plotted in (b); 78 000 solutions! Examination of computed Structural Index (c, d) shows that only a small percentage of solutions have a high SI value. Using SI as a discriminator, and plotting only those solutions with SI > 1 (e) achieves a result where four kimberlites are identified (with tight clusters of solutions), together with an acceptably small number of other potential targets.

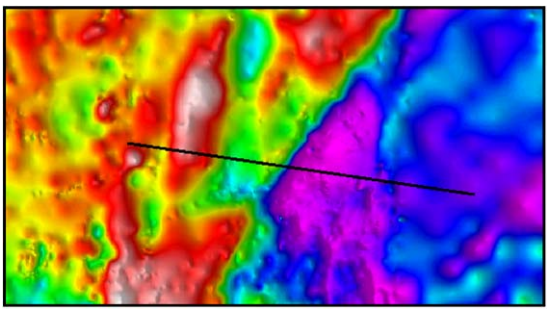

Fig. 4. Image of Bouguer Gravity Anomaly for Renmark Trough area, South Australia, showing location of section line presented in Fig. 5.

Observed data has noise associated with its acquisition and also local distortions of the estimated field introduced by processing. Inappropriate gridding techniques for potential field data such as triangulation, nearest neighbour, cubic interpolation can produce superficially convincing images of the field and its anomalies but violate the continuity of local gradients. The Euler technique breaks down spectacularly for even moderate amounts of artificial Gaussian noise or inappropriate interpolation techniques. This is because the local gradients amplify the non-Laplacian nature of the field. This explains the major difference in behavior for the Euler algorithm between pure analytical model data and real observations.

The model grids for this work were deliberately created directly from the analytical calculated response. This was done to remove any "gridding noise" from the study. Mushayandebvu (2001) has neatly estimated that gridding noise can be estimated by the floor in the eigen value for 2D bodies.

12.2. Conclusions

Euler deconvolution can be applied to gravity data. For simple bodies the SI is one less than the SI for the equivalent magnetic bodies. The contact of significant depth extent does not give rise to a homogeneous gravity

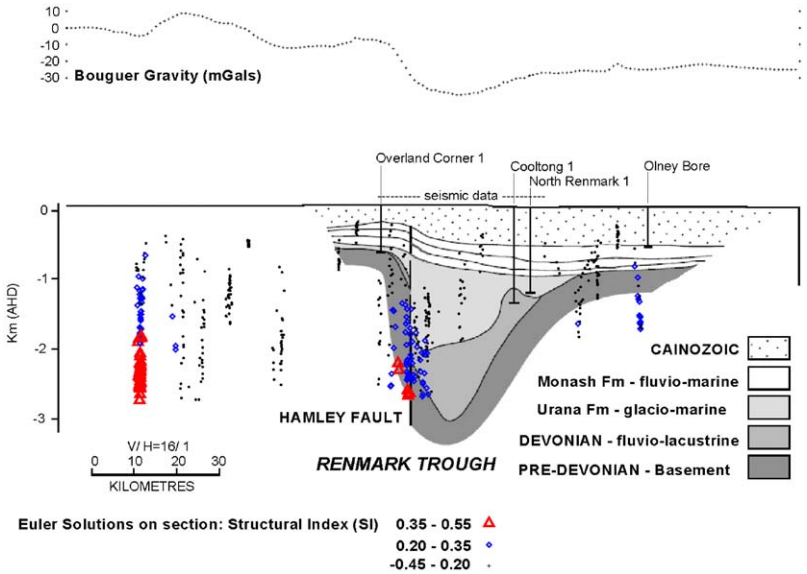

Fig. 5. Section through Renmark Trough, South Australia, showing geology determined from seismic interpretation and drilling in middle part of section. Profile of Bouguer gravity anomaly shows distinct low associated with sedimentary basin. Solutions from Euler deconvolution (two Hilbert equations case)—using solutions from a 2 km wide swath along line of section—are plotted in section view. Again, all solutions have been plotted, with none of traditional discriminators used. Solutions have been classified on basis of computed SI, however, and there is a clear correlation between solutions with higher Structural Index values, and prominent Hamley Fault mapped by seismic data. Based on these results, two other major structures are delineated by Euler solutions.

field and the Euler method is therefore at best an approximation in that case. The two Hilbert equation case is more stable in this situation. Geologically, plausible results are obtained with real data. Discrimination of solutions using depth error estimates is not recommended. The primary quantities X, Y, Z, SI, alpha and beta are more reliably calculated and so should be used for discrimination.

Acknowledgements

The authors would like to thank PIRSA for permission to use the Sheoak Hill and Renmark Trough data. Models were computed using Encom's ModelVision. All Euler work was computed using Intrepid's Euler module. The models and scripts for reproducing this work are available upon request.

References

Hansen, R.O., 2002. 3D Multiple-source Werner deconvolution. Extended Abstracts. SEG 72nd Annual Meeting.

Hansen, R.O., Suciu, L., 2002. Multiple-source Euler deconvolution. Geophysics 67, 525–535.

Mushayandebvu, M.F., van Driel, P., Reid, A.B., Fairhead, J.D., 2001. Magnetic source parameters of two-dimensional structures using extended Euler deconvolution. Geophysics 66, 814–823.

Mushayandebvu, M.F., Lesur, V., Reid, A.B., Fairhead, J.D., 2003. Grid Euler deconvolution with constraints for two-dimensional structures. Geophysics 69, 489–496.

Nabighian, M.N., Hansen, R.O., 2001. Unification of Euler and Werner deconvolution in three dimensions via the generalised Hilbert transform. Geophysics 66, 1805–1810.

Reid, A.B., 2003. Short note: Euler magnetic structural index of a thin bed fault. Geophysics. Published electronically, May 2003.

Reid, A.B., Allsop, J.M., Granser, H., Millett, A.J., Somerton, I.W., 1990. Magnetic interpretation in three dimensions using Euler deconvolution. Geophysics 55, 80–91.

Reid, A.B., FitzGerald, D., McInerney, P., 2003. Euler deconvolution of gravity data. SEG Annual Meeting, Dallas, accepted for presentation.

Stavrev, P.Y., 1997. Euler deconvolution using differential similarity transformations of gravity or magnetic anomalies. Geophysical Prospecting 45, 207–246.

Thompson, D.T., 1982. EULDPH: a new technique for making computer-assisted depth estimates from magnetic data. Geophysics 47, 31–37.

Zhang, C., Mushayandebvu, M.F., Reid, A.B., Fairhead, J.D., Odegard, M.E., 2000. Euler deconvolution of gravity tensor gradient data. Geophysics 65, 512–520.